한국광물학회지 제 14 권 제 1 호 (2001)
J. Miner. Soc. Korea, 14, 31-38 (2001)

Partitioning of Metal Cations During Synthetic Calcite Growth

방해석 결정 성장시 금속 양이온의 분배 현상에 대한 연구

Hyeon Yoon (윤혜온)* · Soo Jin Kim (김수진)**

*Korea Basic Science Institute, 126-16, 5St., Anam-dong, Sungbuk-gu, Seoul 136-701 Korea
(한국기초과학지원연구원, E-mail: dunee@comp.kbsi.re.kr)
**School of Earth and Environmental Sciences, Seoul National University, Seoul 151-742, Korea
(서울대학교 지구환경과학부)

ABSTRACT : The partitioning behavior of common trace metal cations during calcite crystal growth has been examined by means of surface precipitation and continued crystal growing. The pure calcites of A-, B-, and C-type were prepared from 0.02 M, 0.2 M and 0.4 M $CaCl_2 \cdot 2H_2O$ solutions, respectively. The surface morphology of resulting calcite changes depending on solution compositions and growth kinetics. The A-type and B-type exhibit similar surface morphology of simple $\{10\bar{1}4\}$, despite more complicated surface of the B-type. The C-type represents slightly modified surface morphology of $\{01\bar{1}2\}$ face. We examined the surface morphology control of each metal cation during later stage formation of (Ca, Me)CO_3 layer on the pure calcite. In order to distinguish the directional partitioning of metal cation, electron microprobe analysis (EPMA) was performed on three directions on $\{10\bar{1}4\}$ surface. EPMA of the calcite grown with metal cations, (Ca,Me)CO_3 layer, shows that Mn^{2+} and Co^{2+} prefer on $\{01\bar{1}2\}$ and Sr^{2+} prefers on $\{10\bar{1}4\}$. Individual metal cation partitioning in (Ca,Me)CO_3 layers shows following preference orders: Mn^{2+}, C-type > B-type > A-type; Co^{2+}, B-type > A-type > C-type. In addition, Sr^{2+} is exclusively present on the A-type than other two types. EPMA of the three directions on $\{10\bar{1}4\}$ shows little variation for the A-type and B-type except C-type, especially for Mn^{2+} and Co^{2+}.

Keywords : Calcite, Surface Morphology, Trace Metal Cation, Partitioning.

요약 : 방해석 결정 성장시 나타나는 미량금속 양이온의 분배현상을 표면침전 및 연속 결정 성장과정을 통하여 관찰하였다. A, B, C 유형의 순수한 방해석이 각각 3가지 다른 초기 농도 즉 0.02, 0.2, 0.4 M의 $CaCl_2 \cdot 2H_2O$로부터 형성되었으며, 이들의 표면 형태는 합성용액의 조성과 성장 속도에 의해 조절됨을 알 수 있었다. B 유형이 표면형태가 좀더 복잡하지만, A, B 유형은 대체로 단순한 $\{10\bar{1}4\}$면을 가진 방해석과 유사한 표면형태를 보여준다. 이에 반해 C 유형에서는 $\{01\bar{1}2\}$면이 주로 관찰되었다. 순수한 방해석 위에 (Ca,Me)CO_3 층이 형성될 경우에 각 금속 양이온의 표면 형태에 대한 기여도를 관찰하였다. (Ca,Me)CO_3 층의 대해 $\{10\bar{1}4\}$면 3 방향에 대한 전자현미분석 결과 금속 이온의 특징적인 분배현상을 알 수 있었다. Mn^{2+}과 Co^{2+}는 $\{01\bar{1}2\}$에 수직으로, 반면 Sr^{2+}는 $\{10\bar{1}4\}$에 수직 또는 평행한 방향으로 선택적으로 분배되는 현상이 관찰되었다. 합성 방해석 표면 형태에 따른 금속 이온들의 분배 친화도는 Mn^{2+}이 C 유형 > B 유형 > A 유형, 그리고 Co^{2+}은 B 유형 > A 유형 > C 유형이다. 이들 중 Sr^{2+}는 특히 $\{10\bar{1}4\}$면이 잘 발달된 A유형에 더 많은 친화도를 갖는 것으로 나타났다.

주요어 : 방해석, 표면형태, 미량금속이온, 분배현상.

Introduction

Calcite contains a variety of surface sorbed species and coprecipitates, including heavy metal ions, which reflect the mode and environment of their formation and alteration history (Zhong and Mucci, 1995). In geochemical environment, the fate of dissolved metal ions is strongly controlled by interactions with solid surfaces. The processes, by which ions are removed by solid surface, are sorption, coprecipitation, and crystal growth. Therefore, an understanding of fundamental reaction mechanisms between the dissolved species and the solid surface is required to predict their geochemical behavior in natural environments. Calcite-water interactions involving trace metals, and the minor and trace metal concentrations of calcite are commonly used to infer the compositions of surrounding solution and the degree of calcite-water interface reaction (Davis *et al.*, 1987).

Surface reaction processes between calcite and dissolved species are all based on interactions at the mineral-solution interfaces. The surface structure, which can affect the partitioning of metals, has gained considerable attention (Reeder and Grams, 1987; Paquette and Reeder, 1995; Reeder, 1996). The incorporation of trace metals to the calcite has been widespread application to the study of diagenesis/lithification (Mucci and Morse, 1990: Zhong and Mucci, 1995), and surface-reaction-controlled growth mechanism of calcite (Paquette and Reeder, 1995). Experimental studies have been mostly focused either on the study of the preferred partitioning influenced by the growth rate and solution composition (Lorens, 1991), or on the surface structure control of metals distribution in the micro-scale domains of calcite (Paquette and Reeder, 1995; Staudt *et al.*, 1994). The rate-controlled and micro-scale surface-structure-controlled processes have limitation, if the interacting solid exhibits various surface sites for mineral-water interface reaction of metals in natural environments.

In this study, we examined the partitioning behavior of common divalent metal cations, such as Mn^{2+}, Co^{2+}, Sr^{2+} and Mg^{2+}, on the calcite during surface precipitation and subsequent crystal growth processes. This study also points toward the macroscopic examination of the effect of surface morphology on the preferred incorporation of metals during calcite growth.

Experimental Methods

Synthetic calcite crystals were distinguished according to their growth solution compositions as well as growth histories. The first is pure calcite crystal, which was grown from the solutions free of metal ions and the second is the calcite grown from the solution metals.

Pure Calcite Growth

Pure calcite crystals were prepared by a modified version of a free-drift method described by Paquette and Reeder (1995). Three different supersaturating conditions of 0.02 M, 0.2 M, and 0.4 M $CaCl_2 \cdot 2H_2O$ with matching NH_4Cl compositions were selected to control growth rate of calcite crystal and their crystal morphologies. For CO_3 supply to the reaction system, a bottle of $(NH_4)_2CO_3$ was used for introducing CO_2 gas by self dissociation (Paquette and Reeder, 1995). During calcite growth, the system was completely sealed to the atmospheric pCO_2 at constant temperature of 25~27℃ (Fig. 1). The calcite nucleation occurred over periods of 3~4 days and the pH of the solutions

Table 1. Solution chemistry for synthetic calcite growth by free-drift method (unit in mol.).

Calcite type	A-type	B-type	C-type
$Ca^{2+(1)}$	0.02	0.2	0.4
NH^{4+}	0.50	0.80	1.20
Cl^-	0.54	1.20	2.00
pH range(2)	8.7~8.8	8.6~8.7	8.5~8.6

Notes: (1) A-type: 0.02 M, B-type: 0.2 M, and C-type: 0.4 M $CaCl_2 \cdot 2H_2O$.
(2) The range of measured pH values following nucleation.

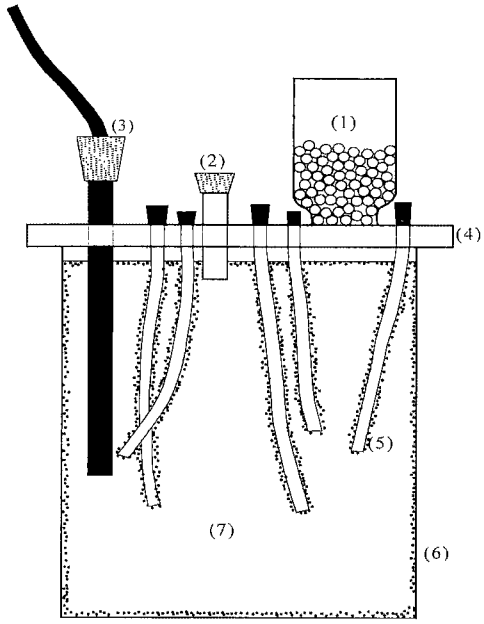

Fig. 1. Schematic diagram of the system used for calcite crystal growth (modified from Gruzensky, 1967). 1) Solid ammonium carbonate sublimates, $(NH_4)_2CO_3$. 2) Port for sampling and doping. 3) pH electrode. 4) Acrylic plate sealing vessel. 5) Tygon tubing used as substrate. 6) Pyrex vessel. 7) Calcium and ammonium chloride solution.

reached about 8.5～8.7. The crystal growth systems were remained 40～50 days until the largest calcite crystals were reached about 150～200 μm in size. The synthetic calcite crystals were classified as A-, B-, and C-type according to their conditions of growth solution (Table 1). At the end of these experiments, each calcite crystal as saved for the subsequent crystal growth with metal cations, such as Mn^{2+}, Co^{2+}, Sr^{2+}, and Mg^{2+}.

(Ca,Me)CO_3 Layer Overgrowth on Pure Calcites

To grow calcite with metal cations, sections of tubing on which the pure calcite crystals of A-, B-, and C-type were already grown from the previous experiment were transferred to the sealed beakers of new growing solutions, $CaCl_2 \cdot 2H_2O$ and NH_4Cl, as described by Paquette and Reeder (1995). The final concentrations of metals for these systems were adjusted to have 1000 ppm for Mn^{2+}, Co^{2+}, and $Sr^{2+}$and 2000 ppm for Mg^{2+} at 0.02 M $CaCl_2 \cdot 2H_2O$. As a result, each sealed beaker have three tygon tubes of different crystal types (A-, B- and C-type calcite) with one metal composition (Table 1). The calcite crystal, which was used in this experiment, was fully-grown showing distinct surface morphology. After 40～50 days of growth with metal cations, the crystals were removed from the system and cleaned immediately in order to reserve original crystal morphology. During (Ca,Me)CO_3 overgrowth, the metal concentration of growth solutions were continuously monitored by removing 1 ml of working solution from the reaction vessel every 5 days. Then, the solution compositions were analysed by ICP-AES (JY 138Ultrace).

EPMA Analysis

Most of calcite crystals overgrown by new (Ca,Me)CO_3 layer growth show the distinct cleavage rhombohedral faces of previous pure seed calcite. However, in some cases, the overgrowth resulted in development of new faces, which can only be recognized by the observation of the cathodoluminescence microscope (CL). Binocular microscope or scanning electron microscope (SEM) observation did not show the characteristic differences on trace metals partitioning. Therefore, preferred partitioning of metal cations was studied by the CL and EPMA.

Preferred partitioning of trace metals on calcite surface was monitored on $\{10\bar{1}4\}$ surface. EPMA was done on three crystallographic directions on the $10\bar{1}4$, ①$\perp\{10\bar{1}4\}$, ②$\perp\{01\bar{1}2\}$, and ③//$\{10\bar{1}4\}$ (Fig. 2). In Fig. 6, three crystallographic directions above mentioned were presented as numbers, A1, A2, or A3, where the first alphabet means A-, B- and C-type, where the second number means the direction of EPMA analysis on $\{10\bar{1}4\}$. Therefore, A1 means the analysis direction ① of the A-type calcite, while A2 means the

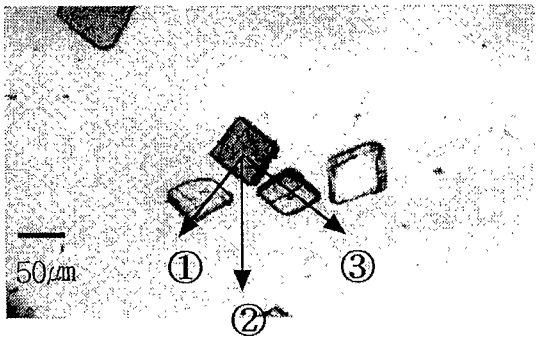

Fig. 2. Electron microprobe analysis directions on synthetic pure calcite surface. ①⊥{10$\bar{1}$4}, ②⊥{01$\bar{1}$2}, and ③//{10$\bar{1}$4}.

analysis direction ② on the A-type calcite.

Atomic Force Microscopy (AFM)

The surface microtopography was studied by AFM. The system used in this study was Auto Probe LS SPM (Park Scientific Instruments) equipped with a 5 μm scanner. It was calibrated using mica at ambient condition in the Department of Chemistry, Chonbuk National University. The cantilevers were Microlevers (Park Scientific Instruments) of force constant of 0.6 N/m with general scan rates of were 12.5 Hz or 25 Hz with height mode. All the samples for AFM experiments were prepared by mounting single calcite crystals (10$\bar{1}$4) face parallel to thin sections. The crystal surface images parallel to corresponding (10$\bar{1}$4) face were recorded.

Results and Discussion

Morphology of Synthetic Crystals

Each of the synthetic calcite crystals, A-, B-, and C-type has characteristic surface morphology. Scanning electron microscope (SEM) show that the synthetic calcite crystals are either twinned or not twinned depending on solution conditions (Fig. 3). SEM observation showed that all three types have the diameter of about 150~200 μm, but distinctive surface morphologies. The A-type and B-type calcite are allrepresent {10$\bar{1}$4} but each crystal of A-type exhibits distinct rhombohedral cleavage while B-type calcite consists of intergrowth of many small crystallites of {10$\bar{1}$4}, complicating the surface morphology of the B-type calcite (Fig. 3). The C-type calcite shows morphology which was modified from {10$\bar{1}$4} faces typically found in highly supersaturated solutions (Paquette and Reeder, 1995).

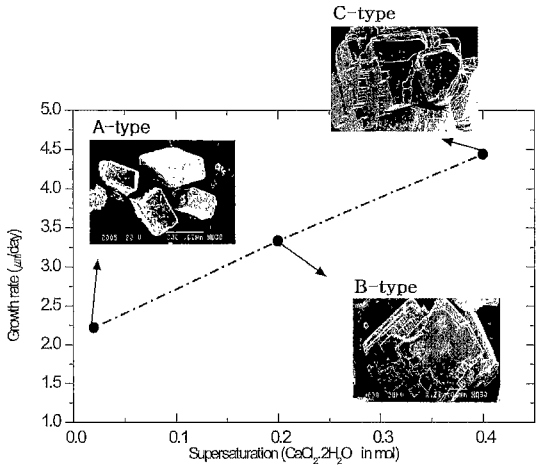

Fig. 3. Morphology of synthetic calcite crystals depending on solution conditions.

AFM Micromorphology of Synthetic Crystals

Large scans (~1 μm) of the calcite crystal surface, {10$\bar{1}$4}, by AFM reveal microtopographic information. The flat terraces are often separated by steps of monolayer height. We examined all the crystal surfaces of A-, B-, and C-types and (Ca,Me)CO_3 layer overgrowth. Each of them shows some regions of fairly homogeneous and ordered crystal face, consisting of characteristic surface (Fig. 4 and 5).

The AFM images show that morphological features of both A-type and C-type are similar but different from the B-type (Fig. 4). Such features were also observed from the two-dimensional surface images, which are not shown in this paper. It is interesting that the pre-existing surface of the A-, B-, and C-type calcite on the

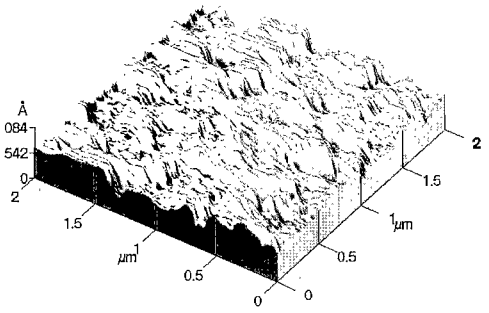

(1) A-type pure calcite

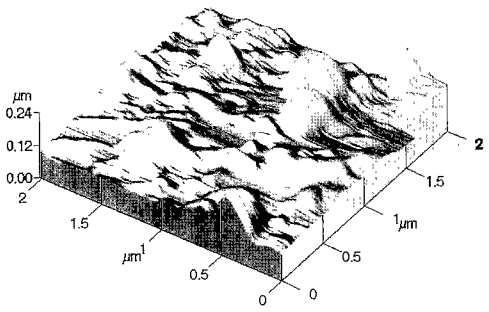

(2) B-type pure calcite

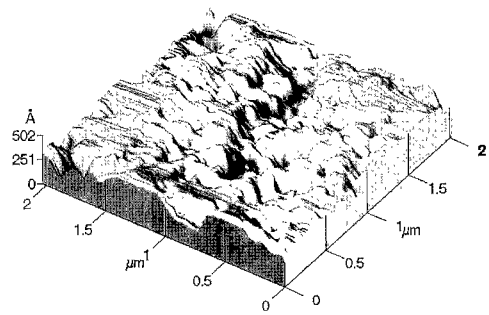

(3) C-type pure calcite

Fig. 4. Surface microtopography by atomic force microscope on $(10\bar{1}4)$ face of A-, B-, and C-type synthetic pure calcite crystals.

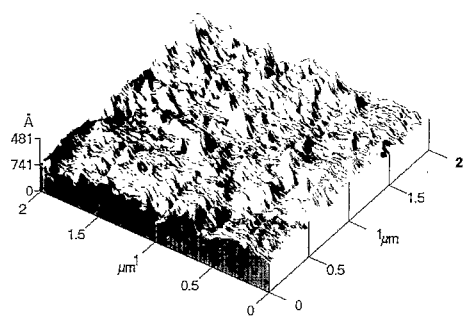

(1) $(Ca,Me)CO_3$ layer growth on pure calcite crystal A

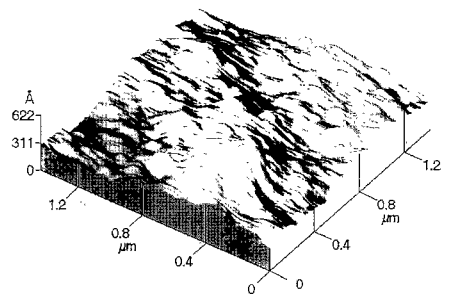

(2) $(Ca,Me)CO_3$ layer growth on pure calcite crystal B

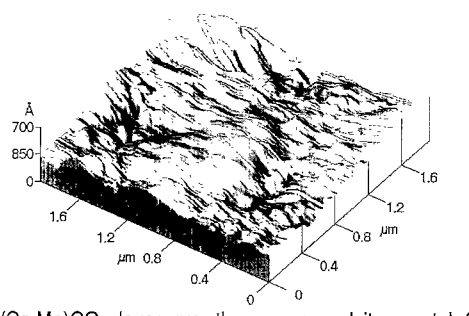

(3) $(Ca,Me)CO_3$ layer growth on pure calcite crystal C

Fig. 5. Surface microtopography by atomic force microscope on $(10\bar{1}4)$ face of $(Ca,Me)CO_3$ layer overgrowth on pure calcite crystals of A-, B-, and C-type. $[Ca]_T$ = 0.02 M and mixed metals concentration was 1000 ppm for each Mn^{2+}, Co^{2+} Sr^{2+}, and Mg^{2+}.

$\{10\bar{1}4\}$ was retained after 45 days of new layer growth of $(Ca,Me)CO_3$ (Fig. 5).

Preferred Partitioning of Metal Cations during $(Ca,Me)CO_3$ Layer Overgrowth

The preferred partitioning of Mn^{2+}, Co^{2+}, Sr^{2+} and Mg^{2+} on the A-, B- and C-type calcites clearly demonstrates surface controlling behavior. The EPMA results show that Mn^{2+} and Mg^{2+} prefer onto the B-type and C-types, and Co^{2+} is highly concentrated on the B-type and A-type calcites (Fig. 6). In C-type calcite, Mn^{2+} is

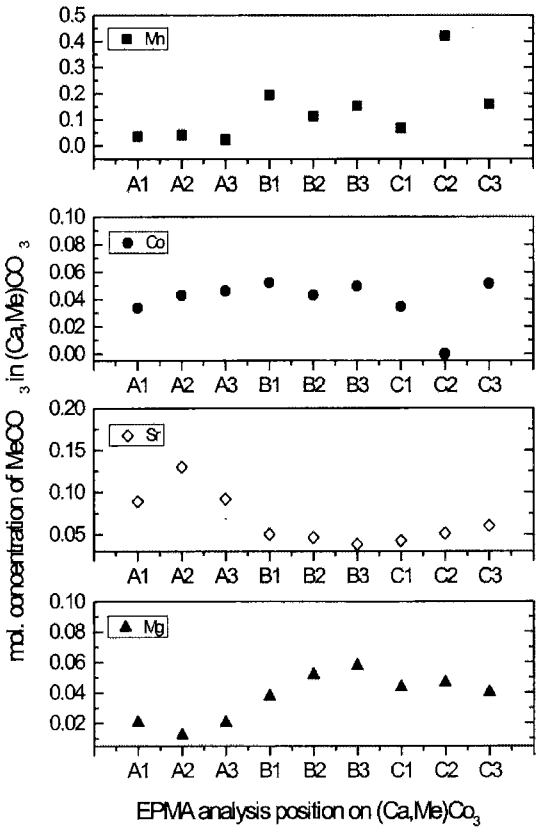

Fig. 6. Electron microprobe analysis data of the $(Ca,Me)CO_3$ layer on pure calcite A-, B- and C-type. (A1; A-type calcite and EPMA analysis direction 1, B2; B-type calcite and EPMA analysis direction 2, C3; C-type calcite and EPMA analysis direction 3). Electron microprobe analysis was done on three crystallographic directions on the $10\bar{1}4$ plane, (1)$\perp\{10\bar{1}4\}$, (2)$\perp\{01\bar{1}2\}$, and (3)// $\{10\bar{1}4\}$.

dominantly presented on the analysis direction $\perp\{01\bar{1}2\}$. Mn^{2+} partitioning in $(Ca,Me)CO_3$ layers shows following orders: C-type > B-type > A-type calcite, while Co^{2+} partitioning on three types of calcite exhibits preferred partitioning order: B-type > A-type > C-type calcite. However, Sr^{2+} is exclusively present on the A-type than other two-types (Fig. 6). EPMA on the three directions on $\{10\bar{1}4\}$ shows little variation for the A-type and B-type calcites, but considerable differences have been found in C-type calcite especially for Mn^{2+} and Co^{2+}.

Effect of Surface Morphology on Trace Metal Partitioning

Surface morphology was examined as a possible control on preferred incorporation of metal cations during calcite growth. Our previous study of trace metal sorption on calcite crystals of different surface morphology demonstrated that the metal sorption is strongly depended and controlled by the surface characters. Although there was a considerable difference in solution compositions between the sorption and surface precipitation and continued crystal growth, we observed same behavior of metal partitioning on calcite surface.

Sr^{2+} concentration on the calcite crystals of rhombohedral $\{10\bar{1}4\}$ shows preferred sorption behavior than on the calcite crystals of $\{01\bar{1}2\}$. Mn^{2+} and Co^{2+} sorption were highly concentrated on the calcite crystals of more complicated surface morphology on which it has many high-energy surface sites such as kinks (Yoon, 2001). According to Titiloye *et al.* (1998), calcite and dolomite surfaces have different surface structures, which have different site energies depending on their crystallographic notations. Atomistic simulation show that $\{10\bar{1}4\}$ on calcite is the most stable face and has the lowest surface energy, while $\{10\bar{1}0\}$ and $\{11\bar{2}0\}$ faces of carbonate minerals have high surface energy (Titiloye *et al.*, 1998). The more stable $\{10\bar{1}4\}$ will behave less favorably for the metals sorption and surface precipitation process. In addition to this, less stable faces of $\{10\bar{1}0\}$ and $\{11\bar{2}0\}$ will behave more favorably during the metal incorporation reactions.

EPMA on the $(Ca,Me)CO_3$ layer growth on pure calcite surface shows different behaviors. Co^{2+} and Mn^{2+} were preferred than Ca^{2+} during surface precipitation process. The apparent partitioning of Mg^{2+} and Sr^{2+} was extremely low compared to that of Mn^{2+} and Co^{2+}. The preferred incorporation of metal cations during surface precipitation reaction also could be explained by the ionic size effect. The effective ionic radii (r_e) of common divalent metal ions have following values, Co^{2+} (0.75 Å), Mn^{2+}

(0.83 Å), Mg^{2+} (0.72 Å), Sr^{2+} (1.18 Å), and Ca^{2+} (1.00 Å) (Shannon, 1976). It is again, likely due to the ionic size of Co^{2+}, which is the smallest of all the trace metals used in this study, that may brought the most preferred partitioning of Co^{2+} during calcite growth. Mn^{2+} shows higher partitioning on the B-type and C-type, but low in A-type. Sr^{2+} has similar ionic radii as Ca^{2+}, but the relative partitioning couldn't be as high as Co^{2+}. Mg^{2+} partitioning is the lowest in all four metal cations used in this study, although the initial concentration of Mg^{2+} was twice as high as compared to the other three metals (Fig. 6). The rhombohedral calcite structure might inhibit higher incorporation of Mg^{2+} on calcite during crystal growth.

Conclusion

The surface morphology was examined to the study of preferred partitioning behavior of metal cations on three types of calcites during (Ca,Me) CO_3 layer overgrowth. Partitioning of trace metals on synthetic calcite demonstrates strong control of surface morphology during calcite growth. The preferred partitioning of metal cations during sorption and continued surface precipitation show same preference. Mn^{2+} and Co^{2+}show higher partitioning on the B-type and C-type, but low in A-type. Sr^{2+} shows high concentration on the A-type calcite of less complicated surface morphology of rhombohedral $\{10\bar{1}4\}$. It seems clear that the calcite surface, whether it has higher energy surface site or not, may prefer to incorporate smaller ions onto its structures. Present study provides an important clue for the understanding of the surface reaction processes, although it has been done in a very simple system. It is also clear that when the trace metal impurities are interacting with the calcite surface, the trace metals partitioning could be regulated not by a single controlling mechanism.

Acknowledgments

We would like to thank Prof. Y. I. Lee and Dr. K. S. Ko for their critical readings of the manuscript and invaluable comments. We would like to thank Dr. S. H. Lee from Korea Basic Science Institute for valuable EPMA analysis. The authors express thank to Dr. H. J. Song from Korea Basic Science Institute, Kwangjoo Branch for valuable SEM images. The authors also would like to thank Prof. G. Y. Jeong and the anonymous reviewer for their critical readings and comments.

References

Davis, J. A., Fuller, C. C., and Cook, A. D. (1987) A model for trace metal sorption processes at the calcite surface: adsorption of Cd^{2+} and subsequent solid solution formation. Geochim. Cosmochim. Acta 51, 1477-1490.

Lorens, R. B. (1991) Sr, Cd, Mn and Co distribution coefficients on calcite as a function of calcite precipitation rate. Geochim. Cosmochim. Acta, 45, 553-561.

Mucci, A. and Morse, J. W. (1990) Chemistry of low-temperature abiotic calcites: Experimental studies on coprecipitation, stability, and fractionation. Rev. Aquatic Sci., 3, 217-254.

Paquette, J. and Reeder, R. J. (1995) Relationship between surface structure, growth mechanism, and trace element incorporation in calcite. Geochim. Cosmochim. Acta, 59, 735-749.

Reeder, R. J. and Grams, J. C. (1987) Sector zoning in calcite cement crystals: implications for trace element distribution coefficient in carbonate. Geochim. Cosmochim. Acta, 51, 187-194.

Reeder, R. J. (1996) Interaction of divalent cobalt, zinc, cadmium, and barium with the calcite surface during layer growth. Geochim. Cosmochim. Acta, 60, 1543-1552.

Shannon, R. D. (1976) Revised effective ionic radii and systematic studies of interatomic distances in halides and chalcogenides. Acta Crystallogr., A32, 751-767.

Stumm, W. and Morgan, J. J. (1996) Aquatic cemistry. 3rd edition, John Wiley & Sons.

Staudt, W. J., Reeder, R. J., and Schoonen, M. A. A., (1994) Surface structure controls on compositional zoning of SO_4^{2-} and SeO_4^{2-} in synthetic calcite single crystals. Geochim. Cosmochim. Acta, 58, 2087-2098.

Titiloye, J. O., de Leeuw, N. H., and Parker, S. C. (1998) Atomistic simulation of the differences between calcite and dolomite surfaces.

Geochim. Cosmochim. Acta, 62, 2637- 2641.

Yoon, H. (2001) A study of metal partitioning in synthetic calcite, Ph. D. Dissertation. Seoul National University. Chapter 4.

Zhong, S. and Mucci, A. (1995) Partitioning of rare earth elements (REEs) between calcite and seawater solutions at 25℃ and 1 atm., and high dissolved metal ions concentrations. Geochim. Cosmochim. Acta, 59, 443-453.

2001년 2월 14일 원고접수, 2001년 3월 7일 게재승인.